Lattice Boltzmann modelling of ionic diffusivity in non-saturated limestone blended cement paste

Cheng Liu, Beatrice Baudet, Mingzhong Zhang*

Department of Civil, Environmental and Geomatic Engineering, University College London, London WC1E 6BT, UK

Abstract: The accurate prediction of ionic diffusivity in non-saturated limestone blended cement paste is essential for the durability design of blended cementitious materials. This paper presents an integrated framework for simulating the ionic diffusivity in limestone blended cement paste considering its 3D microstructure, water saturation level, and distribution of water and gas phases in the pore network. The 3D microstructure of hydrating blended cement paste with various limestone powder (LP) contents and water-to-binder (w/b) ratios was simulated using the voxel-based CEMHYD3D model, based on which a lattice Boltzmann model with in-house codes was employed to simulate the solid-fluid interaction and ionic diffusivity in cement paste. Results indicate that the relative ionic diffusivity in blended cement paste is strongly dependent on the water saturation level, the evolution of which consists of the sharp drop, slow decrease, slight decrease and depercolation periods. For blended cement paste with 10% LP and w/b ratio of 0.5 at 28 d, the change in decrease rate occurs at the critical water saturation levels of 69%, 34% and 7%, respectively. With the increase of w/b ratio and LP content, the relative ionic diffusivity decreases due to the increasing volume fraction and connectivity of capillary pores. However, the relative ionic diffusivity at degrees of saturation above 70% only undergoes a slight decrease from 0.24 to 0.17 with the increasing LP content from 0% to 20%, which can be ascribed to the low reactivity of LP that cannot much modify the pore structure.

Keywords: Limestone filler; Microstructure; Moisture distribution; Diffusion coefficient; Lattice Boltzmann method

1. Introduction

Limestone powder (LP) crushed and ground from natural limestone is one of the base materials for manufacturing Portland cement clinkers. Over the last few decades, LP has been introduced as a supplementary cementitious material to partially replace cement clinker to decrease the CO_2 emissions and improve the sustainability of concrete. The use of LP can help reduce the carbon footprint of concrete by around 15% [1] and decrease the demand for primary raw materials of cement by approximately 10% [2]. Besides, limestone is easily handled and comparatively cheap, the addition of which into cement can help reduce the cost of cement production. Although LP is far less reactive than Portland cement clinkers (even as an inert filler), it would accelerate the rate of hydration of

* Corresponding author. E-mail address: mingzhong.zhang@ucl.ac.uk (M. Zhang)

cement clinkers in blended cement due to the physical effects, e.g., nucleation effect [3]. It can also react with aluminate reaction products from Portland cement to prevent the decomposition of higher volumetric ettringite to lower volumetric monosulphate, i.e. chemical effect [4]. If properly used, the partial replacement of Portland cement clinkers with LP may lead to a denser microstructure of cement paste [5], which would provide a better performance of cementitious materials in terms of mechanical properties and durability [6, 7].

Ionic diffusivity at a saturated state is a critical parameter for assessing the durability and predicting the service life of concrete structures made of limestone blended cementitious materials [8, 9]. Numerous studies have been carried out to investigate the effect of LP on ionic diffusivity in saturated cementitious materials [10-16], concluding that there are several diverse effects to consider in limestone blended cementitious materials. Compared to the reference Portland cementitious materials, the limestone blended cementitious materials are more porous due to the lower reactivity of LP [10]. The aluminate reaction products from Portland cement have a higher binding capacity for ions [11], e.g. chloride ions, but their content in hydrating cement paste is decreased when partially replacing Portland cement with LP. The increasing porosity and decreasing binding capacity for ions lead to an increase in ionic diffusivity in limestone blended cementitious materials. However, such increase can be counteracted by the increasing tortuosity of pores resulting from the aforementioned physical and chemical effects of LP [12-14], which retards the ionic diffusion. Consequently, the influence of LP on ionic diffusivity in cementitious materials is mainly dependent on the dominant factor among them. It is worth noting that in these studies the ionic diffusivity in limestone blended cementitious materials was investigated at a saturated state. However, onsite cementitious materials are partially saturated as a result of self-desiccation [17] and change in the moisture of service environments, e.g. atmospheric and tidal marine conditions [18], and the ionic diffusion is a moisture-dependent process.

There are very few studies on the effect of LP on ionic diffusion in non-saturated cementitious materials, which are mainly focused on the relationship between ionic diffusivity and water saturation level. For instance, de Vera et al. [19] used the natural diffusion method to study the ionic diffusivity in limestone blended concrete at various water saturation levels. They concluded that the ionic diffusivity displays a high dependence on the water saturation level, decreasing by around two orders of magnitude with the decrease of relative humidity from 95% to 54%. Zhang et al. [20] experimentally investigated the effects of LP and slag on ionic diffusivity in non-saturated mortar using the electrical resistivity method. They found that the ionic diffusivity in ternary blended mortar with LP and slag is more sensitive to the decrease of water saturation level than that in pure Portland and slag blended cementitious systems due to the decreasing average pore size and pore connectivity. Ionic diffusion in non-saturated cementitious materials is also associated with the microstructure of

cement paste and moisture distribution in pore network [21], while it is difficult, from experimental measurements, to link the ionic diffusivity in non-saturated blended cementitious materials with their microstructure and moisture distribution in the pore network. Microstructure-based models are useful to reveal the underlying mechanisms of ionic diffusion in partially saturated cementitious materials. Among them, the model proposed by Zhang et al. [22] enables to numerically simulate the water-gas distribution in capillary pore network and the ionic diffusivity in cement paste at various degrees of water saturation. It was indicated that there exists a critical water saturation level between 20% and 34.9%, at which the water-filled pores are disconnected and the ionic diffusion through them cannot occur any more. However, only the ionic diffusivity in non-saturated Portland cement paste was studied and the contribution of gel pores to water saturation level and ionic diffusion was not considered in the model [23-25].

The main purpose of this study is to develop an integrated framework for modelling the ionic diffusivity in non-saturated blended cement paste accounting for its microstructural features and 3D moisture distribution in capillary and gel pores. First, the 3D microstructure of limestone blended cement paste was simulated using CEMHYD3D that is an image-based cement hydration model [26, 27]. The simulated hydration process of limestone blended cement paste, including change in volume fractions of different phases with degree of hydration of clinker and degree of hydration of clinker against curing age, was validated by the modified Powers' model [28] and experimental data. Subsequently, a Lattice Boltzmann (LB) multiphase model was employed to simulate the solid-fluid (water and gas) interaction and equilibrium distribution of water and gas phases in capillary pore network. A LB model for diffusion was then used to predict the ionic diffusivity in blended cement paste with LP contents of 0%, 10%, and 20%, and water-to-binder (w/b) ratios of 0.4, 0.5, and 0.6 at various water saturation levels. The simulation results were compared with experimental data obtained from literature, based on which the underlying mechanisms of ionic diffusion in non-saturated limestone blended cementitious materials were explored and discussed in depth.

2. Modelling of 3D microstructure of limestone blended cement paste

2.1. Hydration model of limestone blended cement

The 3D microstructure of hydrating limestone blended cement paste was simulated using the modified CEMHYD3D model [27], where the chemical and physical effects of LP on the hydration process and microstructural development of cement paste can be simulated according to a cellular automaton-like computer algorithm [26]. To simulate the chemical effect, the monocarboaluminate (AFmc-$C_4A\bar{C}H_{11}$) can be produced in preference to AFm ($C_4A\bar{S}H_{12}$) as $C_4A\bar{S}H_{12}$ is less stable than $C_4A\bar{C}H_{11}$ [4]. The chemical reaction of LP regarded as $CaCO_3$ ($C\bar{C}$) can be expressed as follows [27]:

$$3C_4A\bar{S}H_{12} + 2C\bar{C} + 18H \rightarrow 2C_4A\bar{C}H_{11} + C_6A\bar{S}_3H_{32} \quad (1)$$

where $C_6A\bar{S}_3H_{32}$ is ettringite (AFt-$C_6A\bar{S}_3H_{32}$).

To simulate the physical effects, the precipitation of calcium silicate hydrate (C-S-H) and calcium hydroxide (CH) was allowed on the surface of limestone particles to reflect the nucleation effect of LP. Meanwhile, to simulate the filler effect in blended cement paste, the early time dissolution probabilities of cement clinkers were assumed to be proportional to the ratio of the initial total surface area of binder divided by that of cement clinkers. It has been demonstrated that such modifications are effective for mimicking the physical effects of LP on the hydration process and microstructural evolution of blended cement paste [27]. More details about the CEMHYD3D model can be found in [26, 27]. In this study, the representative volume element (RVE) size of limestone blended cement paste was set as 200 × 200 × 200 μm^3 rather than the commonly used 100 × 100 × 100 μm^3 [29, 30] to avoid the potential size effect that would affect the simulation accuracy [31]. The default resolution of the digital RVE in CEMHYD3D (i.e., 1 μm/voxel) was employed. For the resolution of 1 μm/voxel, the conversion factor that correlates the real-time with computational cycles is 0.00035 h/cycle[2] [27, 32].

In this study, P.I 52.5 Portland cement (equivalent to ASTM Type I cement) was used, the chemical composition and physical properties of which are presented in Table 1, indicating that it is composed of 53.72% C_3S, 24.09% C_2S, 7.61% C_3A, 8.98% C_4AF and extra 5.6% $C\bar{S}H_2$ by volume. The measured particle size distribution of cement is shown in Fig. 1. The intra-particle chemical phase distribution of Portland cement was determined by analysing the scanning electron microscope (SEM) images of well-polished cement powder. The distribution corresponding to the autocorrelation functions of mineral phases is consistent with that reported in [33]. LP was regarded as pure $CaCO_3$ with a density of 2.71 g/cm^3, the particle size distribution of which is also presented in Fig. 1.

2.2. Hydration process of limestone blended cement paste

To validate the hydration process, the simulated volume fractions of phases in hydrating limestone blended cement paste were compared to those predicted using the modified Powers' model [28]. In the original Powers' model, the volume fractions of different phases in Portland cement paste, including capillary pore, unhydrated Portland cement, and hydration products, can be expressed as a function of degree of hydration (DoH) of Portland cement and initial capillary porosity (volume fraction of mixing water in the pre-hydrated cement paste) [34]. Due to the very low reactivity of LP in the binary blended cement, a modified Powers' model [28] that considers LP as an inert filler was later proposed to predict the volume fraction of each component in blended cement paste, as a function of DoH of Portland cement (α), initial capillary porosity (p), and volume fraction of LP in the binder (V_{LP}). In the modified Powers' model, the limestone filler occupies a constant fraction of the system volume and does not participate in the cement hydration. As a result, the volume fractions of reactants and products can be simply reduced by the volume fraction of LP in the system. The detailed equations can be expressed as:

$$V_{cp} = p - 1.32\alpha(1-p)(1-V_{LP}) \quad (2)$$

$$V_{uc} = (1-\alpha)(1-p)(1-V_{LP}) \quad (3)$$

$$V_{hp} = 2.12\alpha(1-p)(1-V_{LP}) \quad (4)$$

$$p = \frac{w/b}{w/b+\frac{1}{SG_b}} \quad (5)$$

$$SG_b = \frac{1}{\frac{1-M_{LP}}{SG_{PC}}+\frac{M_{LP}}{SG_{LP}}} \quad (6)$$

$$V_{LP} = M_{LP}\frac{SG_b}{SG_{LP}} \quad (7)$$

where V_{cp}, V_{uc} and V_{hp} are the volume fractions of capillary pore, unhydrated cement and hydration products respectively, SG_b, SG_{PC} and SG_{LP} denote the specific gravity values of binder, Portland cement and LP respectively, and M_{LP} is the percentage of LP in the blended cement by weight.

Following the modelling procedure of CEMHYD3D, the hydration process of limestone blended cement paste was simulated. Fig. 1 displays the simulated particle size distribution of binders that is in good agreement with the experimental data. Fig. 2 shows a comparison of the simulated and calculated volume fractions of capillary pore and unhydrated Portland cement in limestone blended cement paste using the CEMHYD3D model and modified Powers' model, respectively. Here, the blended cement pastes with three w/b ratios of 0.4, 0.5, and 0.6, and two LP replacement ratios of 0% and 20% were selected for illustration. It can be found that the simulated volume fractions of capillary pore and unhydrated Portland cement both exhibit a linear reduction with DoH. As expected, the higher w/b ratio and LP replacement ratio can lead to a higher ultimate DoH of Portland cement as more water is available [3]. The volume fractions simulated using CEMHYD3D agree well with those calculated using the modified Powers' model, suggesting that the low chemical reactivity of LP has no obvious effect on the overall volume fraction of capillary pore over time. This can be ascribed to the fact that the reaction degree of LP simulated by means of CEMHYD3D is very low, e.g. 5-6% at DoH of 0.90 for the LP, which is close to the measured data for limestone blended cement system with the same mix proportion and similar LP fineness reported by Aqel and Panesar [35].

A comparison between the simulated DoH of Portland cement and the measured data obtained from Bonavetti et al. [36] was carried out, the results of which are shown in Fig. 3. In their experiments, the LP replacement ratios for ASTM type I Portland cement were 0%, 9.3%, and 18.1%, and the fineness of LP used was close to that of Portland cement. It can be observed from the experimental data displayed in Fig. 3 that the DoH of Portland cement dramatically increases within the first 5 d but tends to be stable after that. Besides, the blended cement paste with a higher LP content has a higher DoH for both w/b ratios of 0.4 and 0.5. This is expected since the effective water-to-cement ratio is increased for the blended cement paste with a higher LP content, which can promote the hydration of cement clinker. For the paste with w/b ratio of 0.4, the simulated DoHs of Portland

cement agree well with the measured data. The simulated DoHs of Portland cement for the paste with w/b ratio of 0.5 are slightly lower than the measured data at early curing ages, while both experimental and predicted data follow the same increasing trend and are coincident at 28 d. The slight difference observed can be explained by the fact that the very early hydration process is extremely complicated and the CEMHYD3D model cannot explicitly simulate it due to lack of incorporation of hydration kinetics into the model [26]. In addition, the cement paste with a higher w/b ratio at the early age is inevitable to further hydrate during the sample preparation, which leads to a higher measured DoH of Portland cement [37]. Overall, the hydration process of limestone blended cement system can be simulated using the CEMHYD3D model with acceptable accuracy.

3. Microstructural evolution of limestone blended cement paste

In CEMHYD3D, the microstructure of hydrating limestone blended cement paste is simulated through a series of dissolution, diffusion and reaction cycles that control the movement and transformation of binder voxels. In the simulations, the 3D microstructure at any given curing age can be extracted for visualisation or serving as the input for predicting the properties of hardened cement paste. Fig. 4 shows an example of the microstructural evolution of limestone blended cement paste with 10% LP and w/b ratio of 0.5 till 90 d. With the increase of curing age, the Portland cement particles are gradually consumed, and the hydration products fill the capillary pores, leading to a gradual decrease in capillary porosity and a more tortuous pore structure. The reaction rate of LP is very low compared to Portland cement. For the blended cement paste at 90 d, the spherical LP can still be identified and only the surface of the smaller LP is slightly consumed.

In this study, the 3D microstructure of blended cement pastes with LP replacement ratios of 0%, 10%, and 20%, and w/b ratios of 0.4, 0.5, and 0.6 was generated for simulating the ionic diffusivity in partially saturated paste. It is worth noting that since the digitalised microstructure was employed as the input for predicting ionic diffusivity, the simulation results were highly dependent on the resolution of RVE [38]. Basically, the finest resolution can lead to higher accuracy of simulated transport properties but an increase in computational cost. Garboczi and Bentz [39] demonstrated that for the ionic diffusivity in Portland cement paste, the best resolution is not necessarily the finest resolution, but must be chosen based on the comparison with experiment and various physical length scales present in the cement paste. The accuracy for predicting ionic diffusivity in Portland cement paste using the default resolution, i.e. 1 μm/voxel, has been illustrated in [25, 40-42], and therefore a resolution of 1 μm/voxel was selected here.

4. Modelling of ionic diffusivity in non-saturated limestone blended cement paste

The procedure for modelling the ionic diffusivity in non-saturated limestone blended cement paste includes two steps: the modelling of equilibrium distribution of water and gas phases in pore network, and the modelling of ionic diffusion in cement paste. A multiphase LB model [43] was employed for

the first step, where the capillary pore voxels of the microstructure were randomly converted into liquid and gas voxels based on a pre-set degree of water saturation. According to the attributes of real water-gas distribution including water/gas density ratio and contact angle of water on the surface of solid phases in blended cement paste, a series of input parameters including temperature and virtual density of solid phase were calculated [22]. The multiphase LB modelling procedure consisting of streaming and collision steps was then carried out on the limestone blended cement paste with liquid/gas phases. After obtaining the equilibrium state of liquid/gas distribution, the 3D microstructure of partially saturated limestone blended cement paste was converted into a three-phase domain composed of water-filled capillary pores, C-S-H, and non-diffusive phase including gas-filled capillary pores, unhydrated cement particles, and other crystalline hydration products.

A LB model for diffusion [33] was used for the second step to simulate the ionic diffusion through 3D microstructure and estimate the ionic diffusivity in partially saturated limestone blended cement paste. To simulate the ionic diffusivity, the ionic diffusivity in capillary pore water and C-S-H gel of cement paste as inputs needed to be determined. For capillary pore water, its ionic diffusivity was set as 2.03×10^{-9} m^2/s [43], while the ionic diffusivity in C-S-H is dependent on the degree of water saturation in gel pore network. In a previous study [44], the relationship between ionic diffusivity (D_{CSH}) and degree of water saturation (S_w) in the colloidal C-S-H gel was investigated using the above-mentioned multiphase LB model. In the simulations, the electrical double layer effect on the average ionic diffusivity in gel pores was analytically estimated. It was found that the average ionic diffusivity in gel pores is dominantly dependent on the surface electric potential due to the small range of pore size of colloidal C-S-H gel and was estimated to be around 2.03×10^{-10} m^2/s for C-S-H with low ionic valence electrolyte solution, e.g., NaCl. For C-S-H gel with porosity of 0.28 [45] which is the hydration product from cement clinkers the unsaturated ionic diffusivity can be expressed as:

$$D_{CSH} = D_{CSH,S}(1.29 \cdot S_w^2 - 0.28 \cdot S_w - 0.01) \quad (8)$$

where $D_{CSH,S}$ is the ionic diffusivity in saturated C-S-H, equal to 1.83×10^{-11} m^2/s [44].

After obtaining the pre-set parameters required for the LB model for diffusion, the modelling procedure including collision and streaming steps was iterated until the steady-state diffusion was reached. As the steady-state ionic concentration distribution was acquired, the ionic diffusivity in non-saturated limestone blended cement paste can be calculated according to Fick's first law. The detailed description and validation regarding the LB model for diffusion can be found in [33].

5. Results and discussion

Ionic diffusion in partially saturated cementitious materials is usually estimated using the relative ionic diffusivity, which is defined as the ratio of the ionic diffusivity in the specimen with a given degree of water saturation over that in the saturated specimen [21]. Consequently, both the ionic diffusivity in saturated cement paste and the relative ionic diffusivity in non-saturated cement paste

were modelled, the simulation results of which are presented below in comparison with experimental data from literature.

5.1. Ionic diffusivity in saturated limestone blended cement paste

Taking the microstructure with 10% LP and w/b ratio of 0.5 as an example (see Fig. 4), the steady-state ionic concentration distribution in saturated blended cement pastes at 3, 28 and 90 d is shown in Fig. 5. It can be observed that the ionic distribution becomes more heterogeneous with the increase of curing age as the hydration products gradually fill the capillary pores, which results in a gradual decrease in capillary porosity and a more tortuous capillary pore network. Fig. 6 displays the comparison between simulated and experimental results of ionic diffusivity in saturated limestone blended cement paste at 28 and 56 d. The mix ratios of limestone blended cement paste were chosen to be consistent with those adopted in [14], i.e. w/b ratio of 0.34 with 0% and 15% LP and w/b ratio of 0.37 with 0% and 10% LP. Note that since the test specimen in [14] is concrete, the measured ionic diffusivity in concrete (D_c) was converted into that in cement paste (D_p) using the following equations that can eliminate the dilution and tortuosity effects of aggregate [46]:

$$D_c = \frac{100 - V_{Agg}}{100\tau} D_p \tag{9}$$

$$\tau = \frac{100 + V_{Agg}}{200} \tag{10}$$

where V_{Agg} is the volume fraction of aggregate in concrete which can be calculated according to the mix ratio given in the literature, and τ is the tortuosity of cement paste.

This study is focused on the simulation of ionic natural diffusion, while the experimental data were obtained from electrical migration tests, which were found to be 1.5 to 6 times that measured through natural diffusion cell tests, depending on the difference in chloride concentration between upstream and downstream [47]. In their experiment, Cam and Neithalath [14] used a 2 mol/L NaCl solution and the corresponding contrast ratio was approximately 3 [33]. After conversion, it can be observed that the simulation results are lower than experimental data, but the difference is less than one order of magnitude. This is expected as the cement paste in concrete is more porous than pure bulk paste due to the presence of voids and interfacial transition zone between cement paste and aggregates [48].

The ionic diffusivity in saturated limestone blended cement paste is highly related to its pore structure, including volume fraction and connectivity of capillary pores [49]. Fig. 7 illustrates the relationship between ionic diffusivity and capillary porosity of blended cement pastes with LP contents of 0%, 10%, 20% and 30%, and w/b ratios of 0.4, 0.5 and 0.6. It can be observed that the simulated ionic diffusivity in blended cement paste against capillary porosity follows an exponential function, which is similar to the experimental finding for Portland cement paste [50]. In addition, for a given w/b ratio, the curves of ionic diffusivity for different LP contents look similar and all follow

an exponential growth trend, which can be attributed to the similar pore space accessible for diffusion and the connectivity of capillary pores. This aspect will be discussed in detail below. Moreover, the ionic diffusivity in cement paste as a function of capillary porosity slightly decreases with the increase of w/b ratio, indicating a slight or negligible influence of w/b ratio on the relationship between ionic diffusivity and capillary porosity.

Since the ionic diffusivity in saturated blended cement paste is dependent on not only the capillary porosity but also the connectivity of capillary pores [49], the burning algorithm [26] was implemented to identify the connected and disconnected capillary pores in blended cement paste and then determine the connectivity of capillary pores that is defined as the ratio of the volume of connected capillary pores to the total volume of capillary pores. Fig. 8 shows the evolution of connected (blue) and disconnected capillary pores (red) in the 3D microstructure of blended cement paste with 10% LP and w/b ratio of 0.5, corresponding to that shown in Fig. 4. With the increase of curing age from 3 d to 90 d, the connectivity of capillary pores is decreased from 0.94 to 0.72. The connectivity of capillary pores versus capillary porosity is displayed in Fig. 7, indicating that the change of connectivity of capillary pores with capillary porosity is similar for all limestone blended cement pastes. When the capillary porosity is higher than 0.3, the connectivity changes slightly, oscillating between 0.8 and 1.0, but for the capillary porosity lower than 0.3, the connectivity drops sharply from 0.8 to 0 with decreasing capillary porosity. A depercolation threshold value of about 0.2 capillary porosity corresponding to the zero connectivity for blended cement paste can be observed, which is close to that for Portland cement paste [39]. The similar curves of connectivity of capillary pores versus capillary porosity for cement paste with various LP contents and w/b ratios shown in Fig. 7 indicate that the incorporation of LP has no significant effect on the capillary pore structure of cement paste. This finding can be further confirmed by the relationship between effective ionic diffusivity and effective capillary porosity (i.e., capillary porosity multiplied by connectivity of capillary pores), as shown in Fig. 9. Prior to depercolation of capillary pores (i.e., effective capillary porosity > 0), the logarithmic value of ionic diffusivity versus effective capillary porosity looks approximately linear, regardless of LP content and w/b ratio. It can be attributed to the lower reactivity of LP (reaction degree less than 6% in Section 2) that cannot cause a significant change of capillary pore structure of cement paste [35]. Moreover, as seen in Figs. 7 and 9, after the capillary pores are depercolated, the ionic diffusivity is found to be between 1.0×10^{-12} m^2/s and 4.0×10^{-12} m^2/s, suggesting that the combination of saturated C-S-H network and isolated water-filled capillary pores starts to play an important role in ionic diffusion.

To validate the simulated relationship between ionic diffusivity and capillary porosity, a comparison was carried out with the available experimental data collected from the literature [12, 14-16]. The detailed information on the test samples, curing conditions, and test methods of ionic

diffusivity are summarised in Table 2. Note that for the limestone blended mortar and concrete, the measured ionic diffusivity and capillary porosity were converted into those of cement paste according to the mix ratios listed in the literature. The density of Portland cement, LP and aggregate was assumed to be 3.15 g/cm^3, 2.71 g/cm^3 and 2.6 g/cm^3, respectively. Due to lack of capillary porosity in [12], it was estimated using the modified Powers' model [28] (see Section 2) and DoH of 0.95 for clinkers was assumed considering that the measured blended cement paste with w/b ratio of 0.55 was cured over 150 d [12]. As seen in Fig. 7, the capillary porosity measured from Cam and Neithalath [14] is far higher than other experimental and simulated porosity. It can be ascribed to the fact that different from the capillary porosity measured using mercury intrusion porosimetry in [15, 16], the porosity measured here was determined using the water vacuum saturation method, which accounts for the whole pore volume fraction including voids and capillary and gel pores. The measured data of ionic diffusivity in blended cement paste are found to be well located at both sides of the simulated results. The discrepancy between simulated and experimental data can be attributed to the differences in raw materials, curing conditions, and test methods. A comparison between simulated and experimental ionic diffusivity against curing age and capillary porosity demonstrates that the ionic diffusivity in saturated limestone blended cement paste can be predicted with acceptable accuracy.

5.2. Relative ionic diffusivity in non-saturated limestone blended cement paste

5.2.1. Effect of water saturation level

To obtain the relative ionic diffusivity in non-saturated limestone blended cement paste, the equilibrium distribution of water and gas phases at various degrees of water saturation in capillary pore network was firstly simulated using the multiphase LB model. The water in both capillary and C-S-H gel pores has contributions to the degree of water saturation in cement paste. In addition, as per the Kelvin-Laplace law [37], it can be assumed that with the decrease of water saturation level, the water in capillary pores is first removed, followed by the water in C-S-H gel pores. Taking the blended cement paste with 10% LP and w/b ratio of 0.5 at 28 d, corresponding to the microstructure in Fig. 4c as an example, Figs. 10a and b display the equilibrium distribution of water and gas phases in the microstructure and capillary pore network at degree of water saturation of 77% that includes capillary pore water and C-S-H pore water content. It can be seen that the water tends to fill small capillary pores while the gas phase tends to form gas clusters in blended cement paste, which can be attributed to the hydrophilic surface of cementitious materials, i.e. the wetting angle of water less than 90° [51] (0° in this simulation). Fig. 10c and d show the equilibrium distribution of water in capillary pore network and connected water-filled capillary pores in blended cement paste at degree of water saturation of 77%, respectively. It can be found that most of the water-filled capillary pores are disconnected, with a connectivity of only 0.36.

Treating gas-filled capillary pores as a non-diffusive phase, the LB model for diffusion was used

to simulate the ionic diffusion in non-saturated blended cement paste at various water saturation levels. Fig. 11 shows the steady-state distribution of ionic concentration in blended cement paste with 10% LP and w/b ratio of 0.5 at 28 d and degrees of water saturation of 34%, 77%, and 100%. It can be observed that with the decrease of water saturation level, the channels for ionic diffusion are significantly decreased and become more tortuous. Fig 12 displays the relative ionic diffusivity in blended cement paste with 10% LP and w/b ratio of 0.50 at 28 d against degree of water saturation (circle and line). As can be seen, the relative ionic diffusivity drops with the reduction of water saturation level, the evolution of which can be divided into four periods. First, as the degree of water saturation decreases from 100% to 69%, a sharp reduction in relative ionic diffusivity can be observed from 1.00 to 0.22. Subsequently, the following decreasing degree of water saturation from 69% to 34% leads to a slow decrease in relative ionic diffusivity from 0.22 to 0.07. Afterwards, a slight drop from 0.07 to 0 can be found as the degree of water saturation reduces from 34% to 7%. When the degree of water saturation is less than 7%, the ionic diffusion cannot occur in the pore network of cement paste, i.e., the depercolation takes place.

This changing tendency is directly associated with the distribution of water and gas phases in the pore network of limestone blended cement paste. Due to the relatively higher ionic diffusivity, the water-filled capillary pores play a dominant role in ionic diffusion in blended cement paste [52]. With a decrease of water saturation level, the capillary pore water is gradually removed, which leads to a reduction in effective water-filled capillary porosity. Fig. 13 shows the change of effective water-filled capillary porosity (i.e., water-filled capillary porosity multiplied by connectivity of water-filled capillary pores) as a function of degree of water saturation level. With the decrease of degree of water saturation from 100% to 69%, the effective water-filled capillary porosity is significantly reduced from 0.24 to 0, which can be mainly attributed to the decreasing connectivity of water-filled capillary pores (also see Fig. 13), resulting in a sharp reduction in the curve of relative ionic diffusivity. With a further reduction of degree of water saturation from 69%, the water-filled capillary pores become disconnected, i.e., the depercolation of water-filled capillary pores happens. At that moment, the saturated C-S-H network begins playing a crucial role in ionic diffusion together with disconnected water-filled capillary pores in blended cement paste to provide available diffusion paths [41], as a result of which there exists only a slow decrease in relative ionic diffusivity in cement paste when the degree of water saturation is decreased from 69% to 34%. As the degree of water saturation continues to drop below 34%, all the capillary pores are occupied by gas phase and only the partially saturated C-S-H network contributes to ionic diffusion in blended cement paste. Owing to the relatively low ionic diffusivity in partially saturated C-S-H gel pores (see Eq. (8)), the decreasing tendency of relative ionic diffusivity in blended cement paste is slight for a degree of water saturation less than 34%. When the degree of water saturation reaches 7%, the water-filled gel pores in C-S-H become

disconnected and the depercolation of entire pore network takes place at degree of water saturation of 7%, so that there is no available connected pore path for ionic diffusion in blended cement paste, as seen in the corresponding zero ionic diffusivity in Fig. 12.

5.2.2. Effect of water-to-binder ratio

To investigate the effect of w/b ratio on relative ionic diffusivity in non-saturated limestone blended cement paste, additional simulations were carried out on the blended cement paste with 10% LP and w/b ratios of 0.4 and 0.6 at 28 d. The relative ionic diffusivity in blended cement pastes with w/b ratios of 0.4, 0.5 and 0.6 versus water saturation level is plotted in Fig. 12. It can be seen observed that with the reduction of water saturation level, the decreasing trend of relative ionic diffusivity in blended cement paste with w/b ratios of 0.4 and 0.6 is similar to that with w/b ratio of 0.5. However, for the blended cement paste with a higher w/b ratio, the sharp decrease period with the decrease of degree of water saturation becomes more dramatic, while the following slow decrease period and slight reduction period are less significant. Besides, the relative ionic diffusivity in blended cement paste at a given non-saturated state is decreased with the increase of w/b ratio. For instance, at the degree of water saturation of 77%, the relative ionic diffusivity decreases from 0.46 to 0.25 as the w/b ratio increases from 0.4 to 0.6. These findings can be attributed to the different constituents of pore structure in blended cement paste as a result of various w/b ratios. The fraction of capillary pore volume accounting for the total pore volume (gel pore content plus capillary pore content) [53] and connectivity of capillary pores [54] increase with the increasing w/b ratio, which improves the contribution of the pore network formed by capillary pore water to ionic diffusivity. For instance, as shown in Fig. 13, when the w/b ratio increases from 0.4 to 0.6, the connectivity of capillary pores and effective capillary porosity are respectively increased from 0.48 to 0.85 and from 0.11 to 0.28. This indicates that the role of water-filled capillary pore network in ionic diffusivity becomes more significant for blended cement paste with a higher w/b ratio. Since the water-filled capillary pore network is the dominant channel for ionic diffusion, the relative ionic diffusivity in blended cement paste with a higher w/c ratio at the sharp drop stage is thus more sensitive to the decreasing water saturation degree, while those at the slow and slight decrease stages tend to be less significant.

As seen in Fig. 12, the critical degrees of water saturation for dividing the evolution of relative ionic diffusivity in blended cement paste are found to decrease with the increase of w/b ratio. For example, as the w/b ratio increases from 0.5 to 0.6, the critical degrees of water saturation of blended cement paste are respectively reduced from 69%, 34% and 7% to 66%, 26% and 5%. It can be attributed to the fact that at the same water saturation level, the water-filled porosity in blended cement paste increases with the increase of w/c ratio, which can further increase the connectivity of water-filled capillary pores (see Fig. 13). Taking the blended cement pastes at degree of water saturation of 77% as examples, the capillary pore structure comprised of gas-filled (grey), connected

water-filled (blue) and disconnected water-filled capillary pores (red) is shown in Fig. 14. The corresponding connectivity of water-filled capillary pores and effective water-filled capillary porosity are respectively increased from 0 to 0.65 and from 0 to 0.17 with the increase of w/b ratio from 0.4 to 0.6.

For validation, only limited experimental data of ionic diffusivity in non-saturated limestone blended cementitious materials have been reported until now. de Vera et al. [19] used the natural diffusion method to measure the ionic diffusivity in non-saturated concrete made of CEM II/A-L 32.5 containing around 6%-20% LP with w/b ratio of 0.6. Their experimental data are shown in Fig. 12, where it can be observed that the experimental and simulated results indicate a similar decreasing trend with the reduction of degree of water saturation. However, at high water saturation levels, for a given w/b ratio, the experimental data of relative ionic diffusivity in concrete are slightly greater than the simulated results for blended cement paste, which can be ascribed to the relatively higher porosity of cement paste in concrete compared to pure cement paste due to the presence of voids [55]. As the water saturation level decreases, the water-filled voids in concrete are first removed. The connectivity of water-filled pores of cement paste is not affected, as a result of which the relative ionic diffusivity in concrete at high water saturation levels is less decreased compared to that in cement paste. The experimental data of relative ionic diffusivity in concrete are nevertheless all located in the range of simulated results for blended cement paste with w/b ratios ranging from 0.4 to 0.6.

5.2.3. Effect of replacement ratio of limestone powder

Fig. 15 shows the simulation results of relative ionic diffusivity in blended cement paste with 0%, 10% and 20% LP and w/b ratio of 0.6 at 28 d, indicating that an increase in LP replacement ratio can lead to a slight decrease in relative ionic diffusivity at a given water saturation level. For instance, the relative ionic diffusivity in blended cement paste at degree of water saturation of 70% drops from 0.24 to 0.17 when the LP replacement ratio rises from 0% to 20%. This finding is consistent with that reported by Zhang et al. [20], who confirmed experimentally that higher replacement ratios of supplementary cementitious materials are beneficial to reducing the relative ionic diffusivity in non-saturated blended mortar. The reduction of relative ionic diffusivity in blended cement paste can be attributed to the slight increase in volume fraction and connectivity of capillary pores with the increase of LP content, resulting in a higher sensitivity of relative ionic diffusivity to the decreasing water saturation level. As shown in Fig. 16, when the LP replacement ratio increases from 0% to 20%, the connectivity of capillary pores and effective capillary porosity are both slightly increased from 0.76 to 0.84 and from 0.22 to 0.28, respectively.

The critical degrees of water saturation that divide the change of relative ionic diffusivity in blended cement paste decrease with increasing LP content, which can be explained by the fact that at the same water saturation level, the connectivity of water-filled pores is also increased as the water-

filled porosity increases with the LP content (see Fig. 16). Taking the blended cement paste at degree of water saturation of 77% as an example, the capillary pore network consisting of gas-filled (grey), connected water-filled (blue) and disconnected water-filled capillary pores (red) is shown in Fig. 17. As the LP replacement ratio increases from 0% to 20%, the connectivity of water-filled capillary pores and effective water-filled capillary porosity are increased from 0.24 to 0.44 and from 0.05 to 0.15, respectively. However, due to the lower reactivity of LP [56], the incorporation of LP does not significantly change the complexity of pore structure and chemical attributes of cement paste. Consequently, compared to the effect of w/b ratio discussed in Section 5.2.2, the LP replacement ratio has less influence on the relative ionic diffusivity in blended cement paste with a given w/b ratio.

6. Conclusions

In this study, an integrated framework for modelling the ionic diffusivity in non-saturated limestone blended cement paste was proposed, considering the 3D microstructure and moisture distribution in pore network. The effects of w/b ratio and limestone powder (LP) replacement ratio on ionic diffusivity in blended cement paste with various water saturation levels were, for the first time, investigated. Based on the simulation results in comparison with experimental data obtained from literature, the main conclusions can be drawn as follows:

- The hydration of limestone blended cement simulated using the CEMHYD3D model considering the physical and chemical effects of LP is consistent with that calculated using the modified Powers' model and agrees well with the measured data from the literature. The reaction degree of LP in blended cement paste is low, approximately 5-6%.
- The ionic diffusivity in saturated blended cement paste rises with the increasing LP content, which can be attributed to the increasing capillary porosity induced by the low reactivity of LP. Similar to Portland cement paste, the ionic diffusivity in limestone blended cement paste against capillary porosity follows an exponential function, regardless of w/b ratio and LP replacement ratio. The simulation results of ionic diffusivity in saturated limestone blended cement paste as a function of capillary porosity are in good agreement with experimental data.
- The relative ionic diffusivity in limestone blended cement paste is strongly dependent on the water saturation level, experiencing four periods, i.e., a sharp drop period, a slow decrease period, a slight decrease period, and a non-diffusive period, where the connected water-filled capillary pores, the disconnected water-filled capillary pores together with connected water-filled gel pores in C-S-H, and the connected water-filled gel pores in C-S-H act as the dominant diffusion channels, as well as the depercolation of pore network, respectively. For the blended cement paste with 10% LP and w/b ratio of 0.5 at 28 d, the critical degrees of water saturation for these decrease periods are found to be 69%, 34% and 7%, respectively.
- The relative ionic diffusivity in limestone blended cement paste at a given water saturation level

is significantly increased with the decrease of w/b ratio that results in an obvious reduction in porosity and connectivity of capillary pores. However, the relative ionic diffusivity is only slightly decreased with the increase of LP replacement ratio as the low reactivity of LP cannot lead to a significant change in pore structure and hydration products.

This study is mainly focused on the effect of microstructure on ionic diffusivity in non-saturated limestone blended cement paste. It should be noted that the incorporation of LP into a cement system would alter its pore solution and thus may affect the ionic diffusion in cementitious materials considering the changing electrical double layer effect with the ionic concentration of pore solution [57]. Therefore, it is important to estimate such effect on ionic diffusivity in limestone blended concrete. This is a subject of ongoing work and will be presented in a future publication.

Acknowledgements

The authors gratefully acknowledge the financial support from the Engineering and Physical Sciences Research Council (EPSRC), UK under Grant No. EP/R041504/1 and the Royal Society, UK under Award No. IEC\NSFC\191417 as well as the Visiting Researcher Fund Program of State Key Laboratory of Water Resources and Hydropower Engineering Science, China under Award No. 2019SGG01. The financial support provided by University College London (UCL) and China Scholarship Council (CSC) to the first author is also greatly acknowledged.

References

[1] A.A. Elgalhud, R.K. Dhir, G. Ghataora, Limestone addition effects on concrete porosity, Cement and Concrete Composites, 72 (2016) 222-234.

[2] M. Schmidt, Cement with interground additives-capabilities and environmental relief: I, ZKG International, Edition B, 45 (1992) 64-69.

[3] D. Wang, C. Shi, N. Farzadnia, Z. Shi, H. Jia, Z. Ou, A review on use of limestone powder in cement-based materials: Mechanism, hydration and microstructures, Construction and Building Materials, 181 (2018) 659-672.

[4] H.-J. Kuzel, H. Pöllmann, Hydration of C3A in the presence of $Ca(OH)_2$, $CaSO_4 \cdot 2H_2O$ and $CaCO_3$, Cement and Concrete Research, 21 (1991) 885-895.

[5] K. De Weerdt, M.B. Haha, G. Le Saout, K.O. Kjellsen, H. Justnes, B. Lothenbach, Hydration mechanisms of ternary Portland cements containing limestone powder and fly ash, Cement and Concrete Research, 41 (2011) 279-291.

[6] W. Zhu, J.C. Gibbs, Use of different limestone and chalk powders in self-compacting concrete, Cement and Concrete Research, 35 (2005) 1457-1462.

[7] K. Vance, M. Aguayo, T. Oey, G. Sant, N. Neithalath, Hydration and strength development in ternary portland cement blends containing limestone and fly ash or metakaolin, Cement and Concrete Composites, 39 (2013) 93-103.

[8] R.A. Patel, Q.T. Phung, S.C. Seetharam, J. Perko, D. Jacques, N. Maes, G. De Schutter, G. Ye, K. Van Breugel, Diffusivity of saturated ordinary Portland cement-based materials: A critical review of experimental and analytical modelling approaches, Cement and Concrete Research, 90 (2016) 52-72.
[9] C. Liu, R. Qian, G. Liu, M. Zhang, Y. Zhang, Three-dimensional modeling of transport properties in hardened cement paste using metal centrifugation-based pore network, Journal of Materials in Civil Engineering, 33 (2021) 04021361.
[10] P. Silva, J. de Brito, Experimental study on chloride migration coefficients of SCC with binary and ternary mixtures of fly ash and limestone filler, UKIERI Concrete Congress: Innovations in Concrete Construction, Jalandhar (Punjab), India. National Institute of Technology, Engineering College, 2013, pp. 5-8.
[11] F. Lollini, E. Redaelli, L. Bertolini, Effects of portland cement replacement with limestone on the properties of hardened concrete, Cement and Concrete Composites, 46 (2014) 32-40.
[12] H. Hornain, J. Marchand, V. Duhot, M. Moranville-Regourd, Diffusion of chloride ions in limestone filler blended cement pastes and mortars, Cement and Concrete Research, 25 (1995) 1667-1678.
[13] M.S. Meddah, M.C. Lmbachiya, R.K. Dhir, Potential use of binary and composite limestone cements in concrete production, Construction and Building Materials, 58 (2014) 193-205.
[14] H.T. Cam, N. Neithalath, Moisture and ionic transport in concretes containing coarse limestone powder, Cement and Concrete Composites, 32 (2010) 486-496.
[15] Q.T. Phung, N. Maes, E. Jacops, D. Jacques, G. De Schutter, G. Ye, Insights and issues on the correlation between diffusion and microstructure of saturated cement pastes, Cement and Concrete Composites, 96 (2019) 106-117.
[16] C. Li, L. Jiang, N. Xu, S. Jiang, Pore structure and permeability of concrete with high volume of limestone powder addition, Powder Technology, 338 (2018) 416-424.
[17] J.-K. Kim, C.-S. Lee, Moisture diffusion of concrete considering self-desiccation at early ages, Cement and Concrete Research, 29 (1999) 1921-1927.
[18] C. Zhou, F. Ren, Q. Zeng, L. Xiao, W. Wang, Pore-size resolved water vapor adsorption kinetics of white cement mortars as viewed from proton NMR relaxation, Cement and Concrete Research, 105 (2018) 31-43.
[19] G. de Vera, M.A. Climent, E. Viqueira, C. Antón, C. Andrade, A test method for measuring chloride diffusion coefficients through partially saturated concrete. Part II: The instantaneous plane source diffusion case with chloride binding consideration, Cement and Concrete Research, 37 (2007) 714-724.
[20] Y. Zhang, Z. Yang, G. Ye, Dependence of unsaturated chloride diffusion on the pore structure

in cementitious materials, Cement and Concrete Research, 127 (2020) 105919.
[21] Y. Zhang, M. Zhang, Transport properties in unsaturated cement-based materials–A review, Construction and Building Materials, 72 (2014) 367-379.
[22] M. Zhang, G. Ye, K. van Breugel, Modeling of ionic diffusivity in non-saturated cement-based materials using lattice Boltzmann method, Cement and Concrete Research, 42 (2012) 1524-1533.
[23] D. Hou, Y. Jia, J. Yu, P. Wang, Q. Liu, Transport properties of sulfate and chloride ions confined between calcium silicate hydrate surfaces: a molecular dynamics study, The Journal of Physical Chemistry C, 122 (2018) 28021-28032.
[24] P.J. McDonald, V. Rodin, A. Valori, Characterisation of intra-and inter-C–S–H gel pore water in white cement based on an analysis of NMR signal amplitudes as a function of water content, Cement and Concrete Research, 40 (2010) 1656-1663.
[25] R.A. Patel, J. Perko, D. Jacques, G. De Schutter, G. Ye, K. Van Bruegel, Effective diffusivity of cement pastes from virtual microstructures: Role of gel porosity and capillary pore percolation, Construction and Building Materials, 165 (2018) 833-845.
[26] D.P. Bentz, Three-dimensional computer simulation of Portland cement hydration and microstructure development, Journal of the American Ceramic Society, 80 (1997) 3-21.
[27] D. Bentz, Modeling the influence of limestone filler on cement hydration using CEMHYD3D, Cement and Concrete Composites, 28 (2006) 124-129.
[28] E.I. Nadelman, K.E. Kurtis, Application of Powers' model to modern portland and portland limestone cement pastes, Journal of the American Ceramic Society, 100 (2017) 4219-4231.
[29] Y. Gao, G. De Schutter, G. Ye, Z. Tan, K. Wu, The ITZ microstructure, thickness and porosity in blended cementitious composite: Effects of curing age, water to binder ratio and aggregate content, Composites Part B: Engineering, 60 (2014) 1-13.
[30] S. Bishnoi, S. Joseph, A. Kaur, Microstructural modelling of the strength of mortars containing fly ash using μic, Construction and Building Materials, 163 (2018) 912-920.
[31] M. Zhang, G. Ye, K. Van Breugel, A numerical-statistical approach to determining the representative elementary volume (REV) of cement paste for measuring diffusivity, Materiales de Construcción, 60 (2010) 7-20.
[32] C. Liu, M. Zhang, Effect of curing temperature on hydration, microstructure and ionic diffusivity of fly ash blended cement paste: A modelling study, Construction and Building Materials, 297 (2021) 123834.
[33] C. Liu, F. Wang, M. Zhang, Modelling of 3D microstructure and effective diffusivity of fly ash blended cement paste, Cement and Concrete Composites, (2020) 103586.
[34] T.C. Powers, T.L. Brownyard, Studies of the physical properties of hardened Portland cement paste, Journal Proceedings, 1946, pp. 101-132.

[35] M. Aqel, D. Panesar, Hydration kinetics and compressive strength of steam-cured cement pastes and mortars containing limestone filler, Construction and Building Materials, 113 (2016) 359-368.
[36] V. Bonavetti, H. Donza, G. Menendez, O. Cabrera, E. Irassar, Limestone filler cement in low w/c concrete: A rational use of energy, Cement and Concrete Research, 33 (2003) 865-871.
[37] K. Li, M. Stroeven, P. Stroeven, L.J. Sluys, Effects of technological parameters on permeability estimation of partially saturated cement paste by a DEM approach, Cement and Concrete Composites, 84 (2017) 222-231.
[38] S.D. Abyaneh, H. Wong, N. Buenfeld, Modelling the diffusivity of mortar and concrete using a three-dimensional mesostructure with several aggregate shapes, Computational Materials Science, 78 (2013) 63-73.
[39] E.J. Garboczi, D.P. Bentz, The effect of statistical fluctuation, finite size error, and digital resolution on the phase percolation and transport properties of the NIST cement hydration model, Cement and Concrete Research, 31 (2001) 1501-1514.
[40] E.J. Garboczi, D.P. Bentz, Multiscale analytical/numerical theory of the diffusivity of concrete, Advanced Cement Based Materials, 8 (1998) 77-88.
[41] Y. Yang, M. Wang, Pore-scale modeling of chloride ion diffusion in cement microstructures, Cement and Concrete Composites, 85 (2018) 92-104.
[42] S. Kamali-Bernard, F. Bernard, W. Prince, Computer modelling of tritiated water diffusion test for cement based materials, Computational Materials Science, 45 (2009) 528-535.
[43] R.A. Robinson, Stokes, RH Electrolyte Solutions, London, Butterworths Scientific Publications, 19550 (1959) 540-544.
[44] C. Liu, M. Zhang, Microstructure-based modelling of ionic diffusivity in non-saturated cement paste accounting for capillary and gel pores, Submitted to Cement and Concrete Research, (2021).
[45] T.C. Powers, Structure and physical properties of hardened Portland cement paste, Journal of the American Ceramic Society, 41 (1958) 1-6.
[46] A. Hamami, P. Turcry, A. Aït-Mokhtar, Influence of mix proportions on microstructure and gas permeability of cement pastes and mortars, Cement and Concrete Research, 42 (2012) 490-498.
[47] M. Castellote, C. Andrade, C. Alonso, Measurement of the steady and non-steady-state chloride diffusion coefficients in a migration test by means of monitoring the conductivity in the anolyte chamber. Comparison with natural diffusion tests, Cement and Concrete Research, 31 (2001) 1411-1420.
[48] N. Olsson, V. Baroghel-Bouny, L.-O. Nilsson, M. Thiery, Non-saturated ion diffusion in concrete–A new approach to evaluate conductivity measurements, Cement and Concrete Composites, 40 (2013) 40-47.
[49] C. Liu, C. Qian, R. Qian, Z. Liu, H. Qiao, Y. Zhang, Numerical prediction of effective diffusivity

in hardened cement paste between aggregates using different shapes of cement powder, Construction and Building Materials, 223 (2019) 806-816.
[50] S. Numata, H. Amano, K. Minami, Diffusion of tritiated water in cement materials, Journal of Nuclear Materials, 171 (1990) 373-380.
[51] T. Hutzenlaub, J. Becker, R. Zengerle, S. Thiele, Modelling the water distribution within a hydrophilic and hydrophobic 3D reconstructed cathode catalyst layer of a proton exchange membrane fuel cell, Journal of Power Sources, 227 (2013) 260-266.
[52] E. Garboczi, D. Bentz, Computer simulation of the diffusivity of cement-based materials, Journal of materials science, 27 (1992) 2083-2092.
[53] Q. Zeng, K. Li, T. Fen-Chong, P. Dangla, Pore structure characterization of cement pastes blended with high-volume fly-ash, Cement and Concrete Research, 42 (2012) 194-204.
[54] K. Kurumisawa, K. Tanaka, Three-dimensional visualization of pore structure in hardened cement paste by the gallium intrusion technique, Cement and concrete research, 36 (2006) 330-336.
[55] H. Wong, A. Pappas, R. Zimmerman, N. Buenfeld, Effect of entrained air voids on the microstructure and mass transport properties of concrete, Cement and Concrete Research, 41 (2011) 1067-1077.
[56] S. Liu, Y. Kong, L. Wang, A comparison of hydration properties of cement–low quality fly ash binder and cement–limestone powder binder, Journal of Thermal Analysis and Calorimetry, 116 (2014) 937-943.
[57] L. Nachbaur, P.-C. Nkinamubanzi, A. Nonat, J.-C. Mutin, Electrokinetic properties which control the coagulation of silicate cement suspensions during early age hydration, Journal of Colloid and Interface Science, 202 (1998) 261-268.

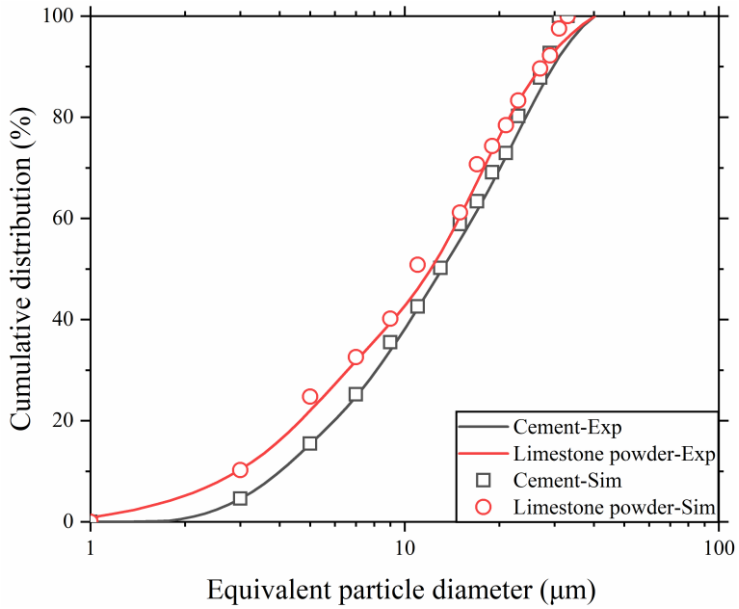

Fig. 1. Particle size distribution of cement and limestone powder.

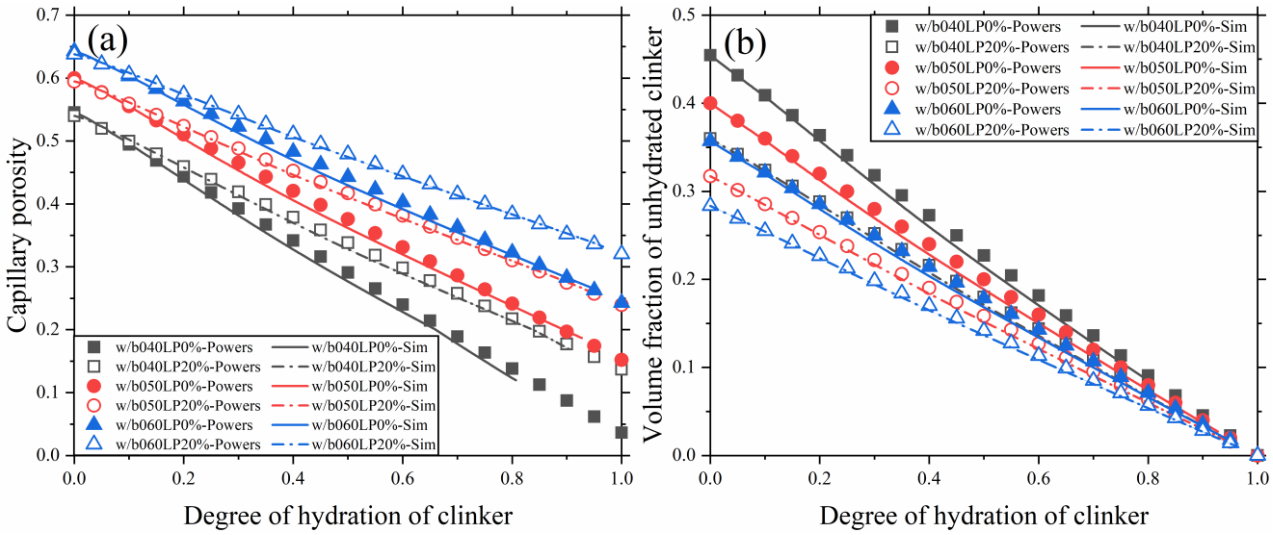

Fig. 2. Change of capillary porosity (a) and volume fraction of unhydrated clinker (b) with degree of hydration of clinker in limestone blended cement paste calculated using modified Powers' equations and simulated using CEMHYD3D.

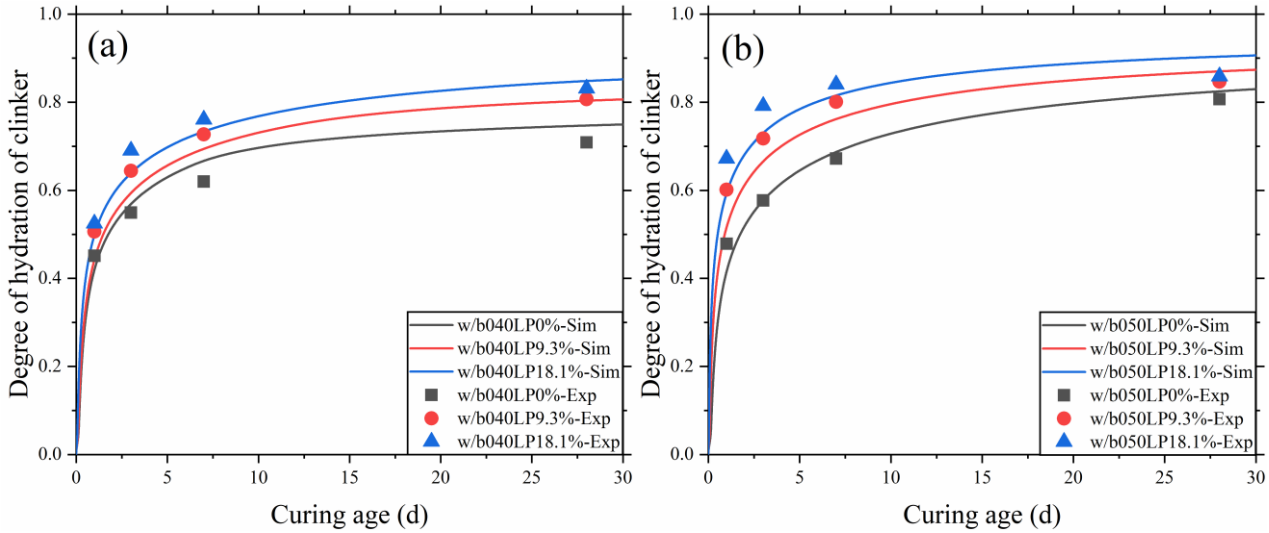

Fig. 3. Comparison between the simulated and measured degree of hydration of clinker in limestone blended cement pastes with w/b ratios of 0.4 (a) and 0.5 (b) after [36].

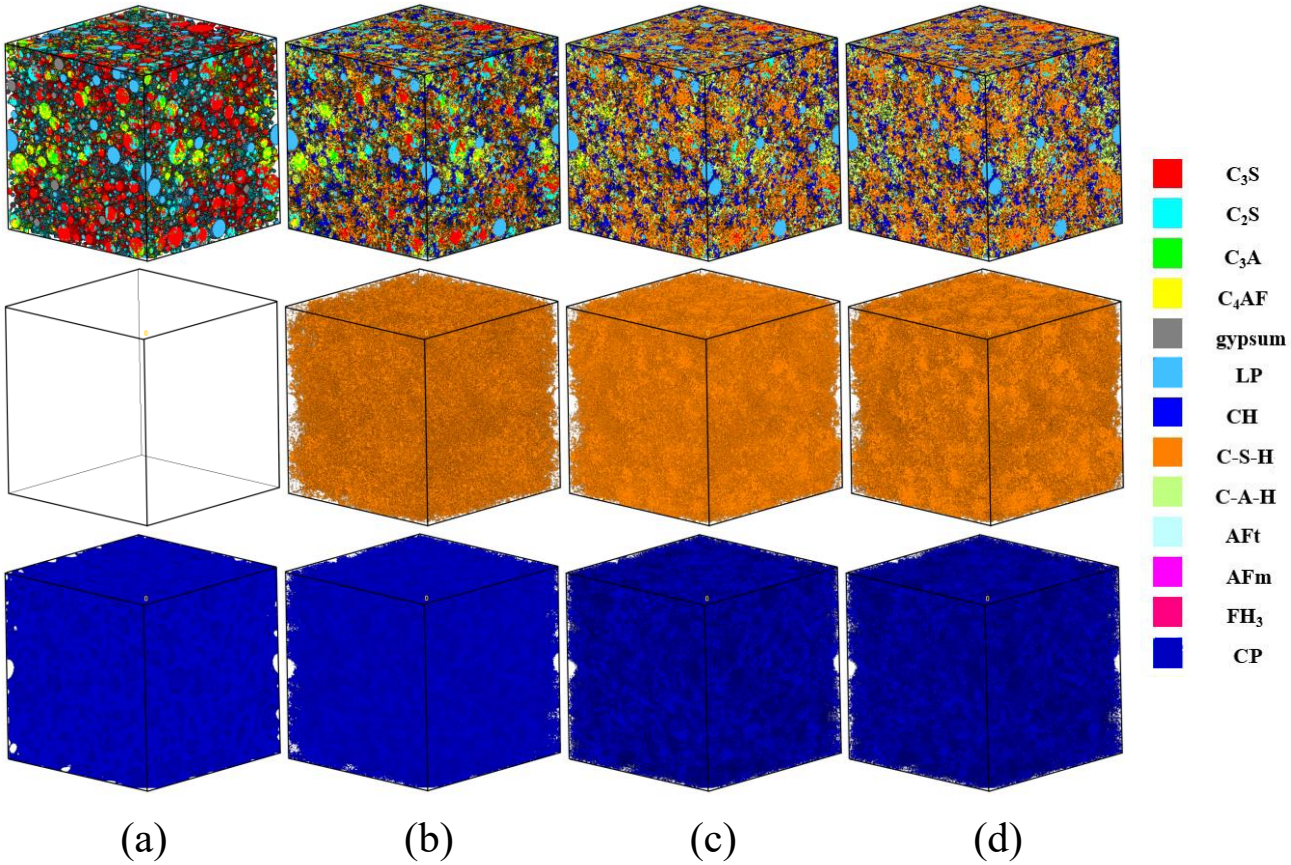

Fig. 4. Microstructural evolution of blended cement paste with 10% limestone powder (LP) and w/b ratio of 0.5 at 0 d (a), 3 d (b), 28 d (c), and 90 d (d) (top row – solid, middle row – C-S-H, bottom row – capillary pore).

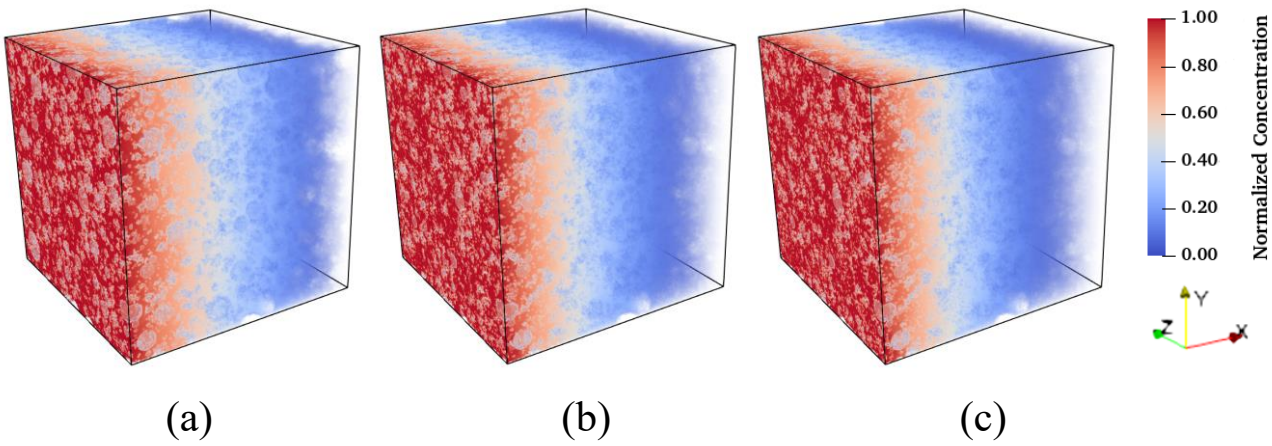

Fig. 5. Steady-state distribution of ionic concentration in saturated blended cement paste with 10% limestone powder and w/b ratio of 0.5 at 3 d (a), 28 d (b), and 90 d (c).

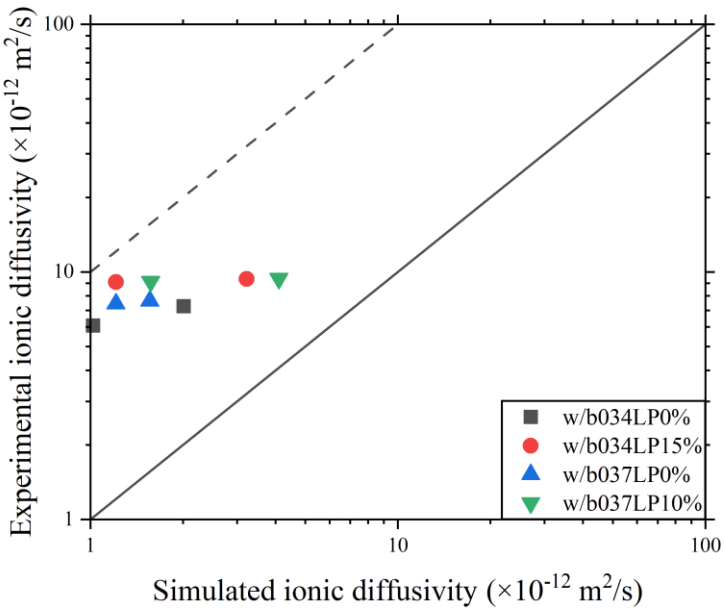

Fig. 6. Comparison between simulated and experimental results of ionic diffusivity in saturated limestone blended cement paste at 28 and 56 d [14].

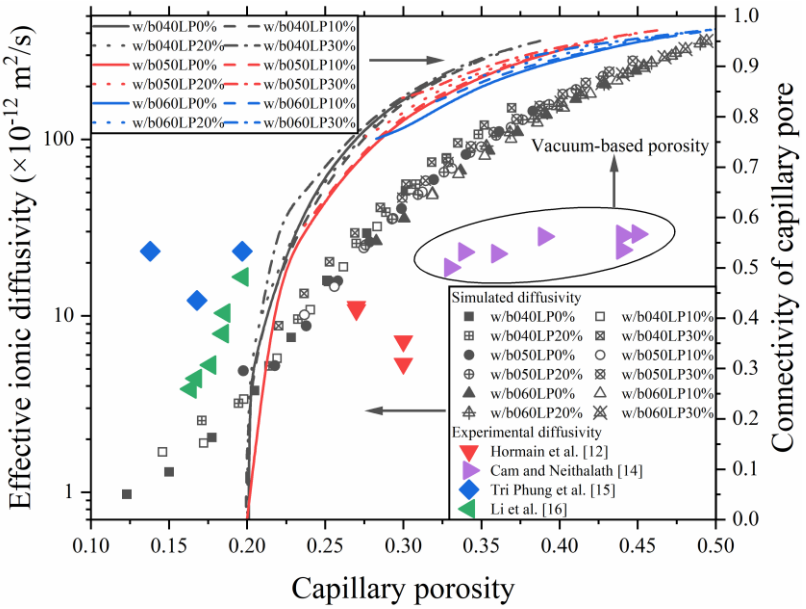

Fig. 7. Effective ionic diffusivity and connectivity of capillary pore in relation to capillary porosity of saturated limestone blended cement paste.

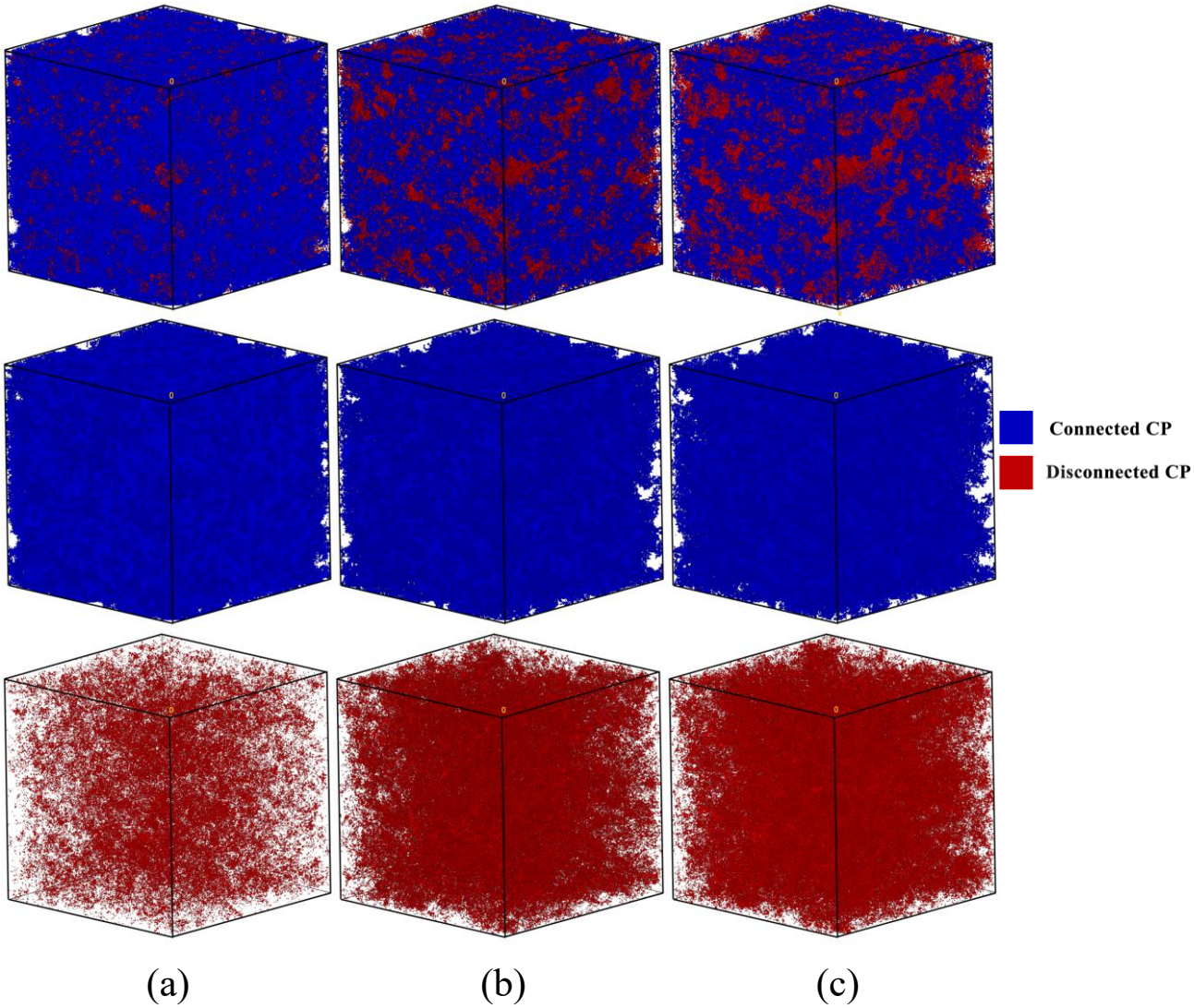

Fig. 8. Connected (blue) and disconnected (red) capillary pore network of blended cement paste with 10% limestone powder and w/b ratio of 0.5 at 3 d (a), 28 d (b), and 90 d (c).

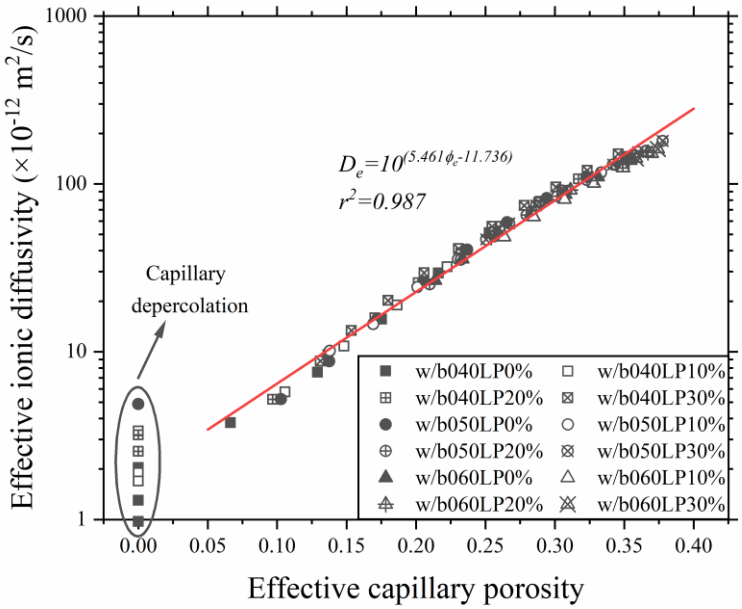

Fig. 9. Relationship between effective ionic diffusivity and effective capillary porosity of saturated limestone blended cement paste.

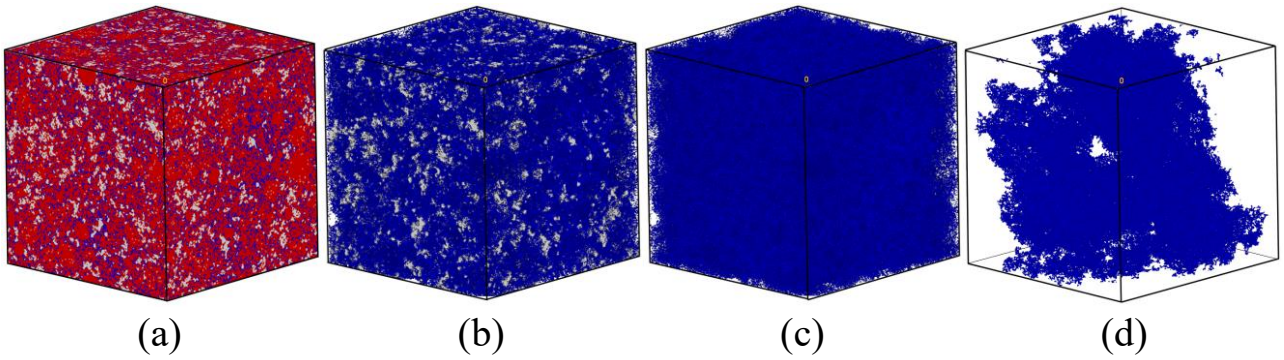

Fig. 10. Equilibrium distribution of water and gas phases in microstructure (a) and capillary pore network (b); water-filled capillary pores (c) and connected water-filled capillary pores (d) in blended cement paste with 10% limestone powder, w/b ratio of 0.5, and degree of water saturation of 77% at 28 d (Blue, grey and red colours represent water, gas and solid phases, respectively)

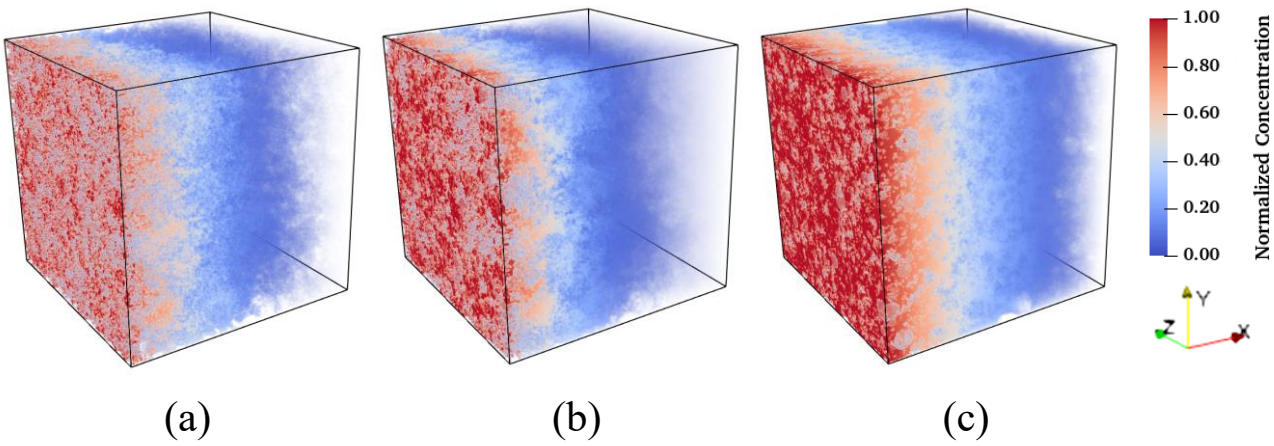

Fig. 11. Steady-state distribution of ionic concentration in blended cement paste with 10% limestone powder, w/b ratio of 0.5, and degrees of water saturation of 34% (a), 77% (b) and 100% (c) at 28 d along *X*-direction.

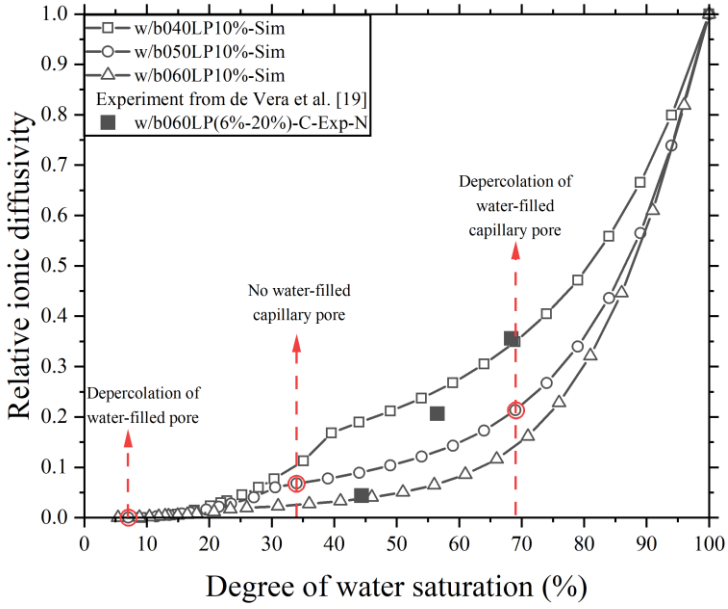

Fig. 12. Relationship between relative ionic diffusivity and degree of water saturation in blended cement paste with 10% limestone powder and w/b ratios of 0.4, 0.5 and 0.6 at 28 d.

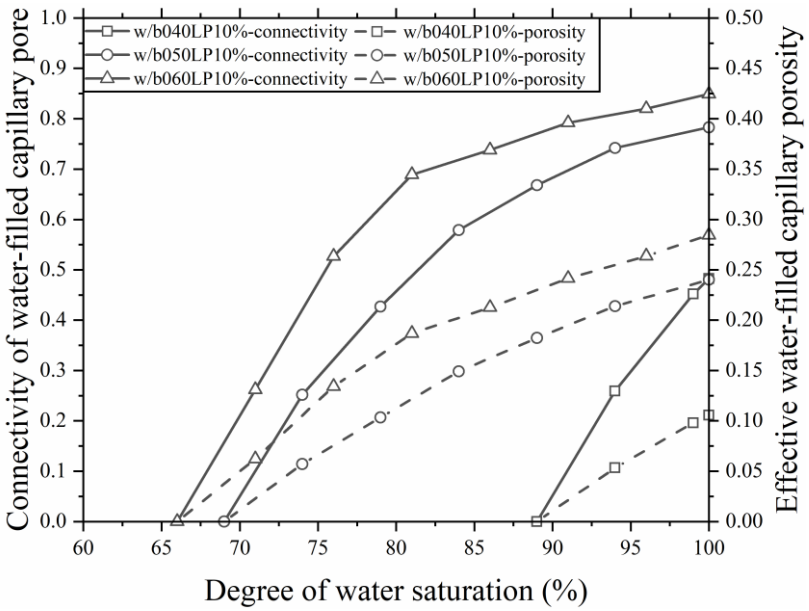

Fig. 13. Connectivity of water-filled capillary pores and effective water-filled capillary porosity against degree of water saturation in blended cement paste with 10% 10% limestone powder and w/b ratios of 0.4, 0.5 and 0.6 at 28 d.

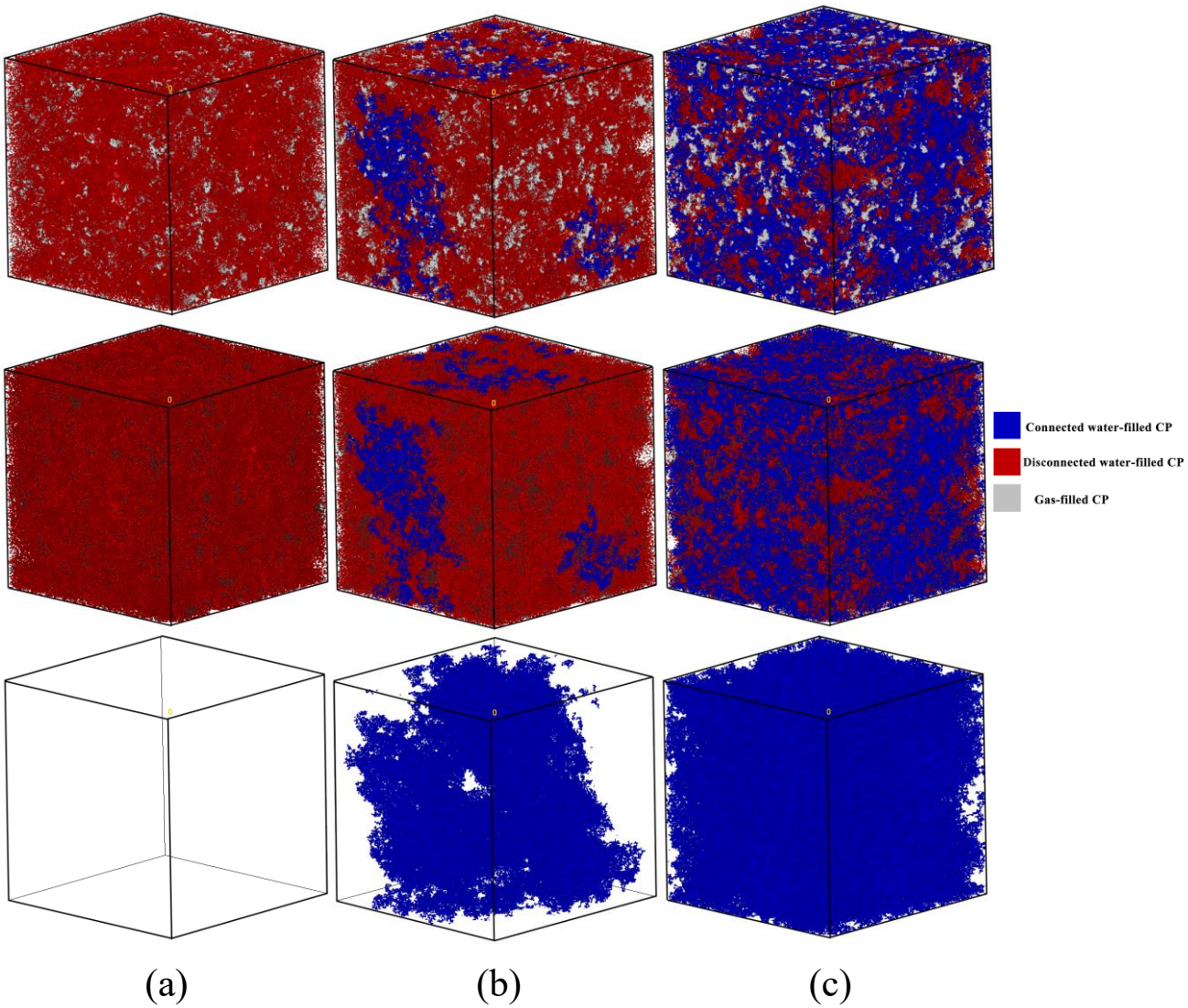

Fig. 14. Capillary pore structure consisting of gas-filled (grey), connected water-filled (blue), and

disconnected water-filled capillary pores (red) in blended cement paste with 10% limestone powder, w/b ratios of 0.4 (a), 0.5 (b) and 0.6 (c), and degree of water saturation of 77% at 28 d.

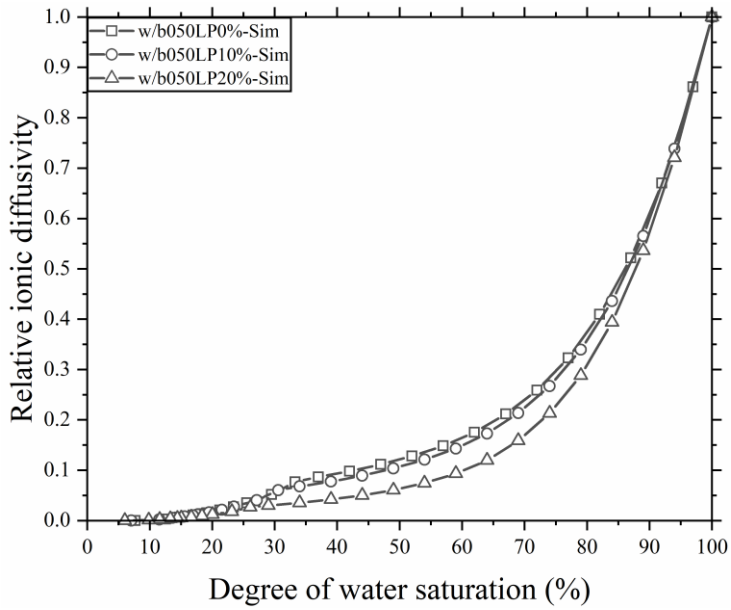

Fig. 15. Relationship between relative ionic diffusivity and degree of water saturation in blended cement paste with 0%, 10% and 20% 10% limestone powder, and w/b ratio of 0.5 at 28 d.

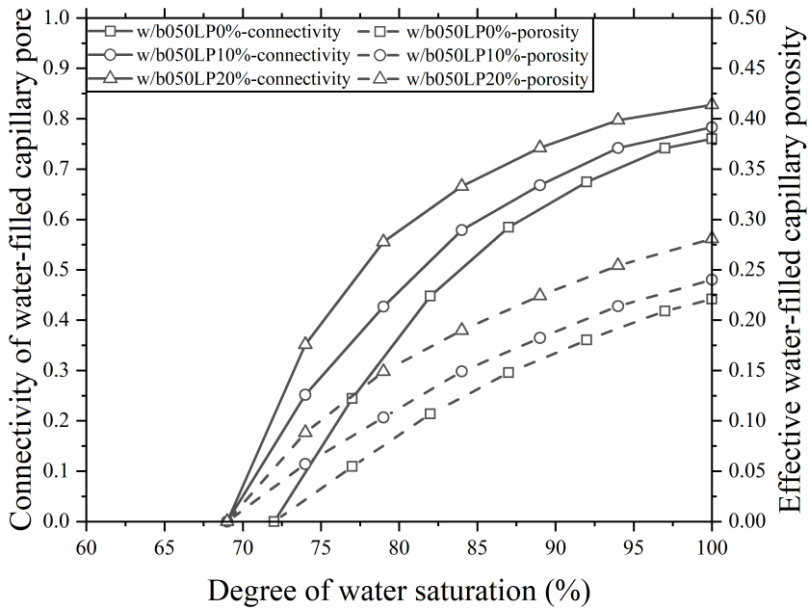

Fig. 16. Connectivity of water-filled capillary pores and effective water-filled capillary porosity against degree of water saturation in blended cement paste with 0%, 10% and 20% 10% limestone powder, and w/b ratio of 0.5 at 28 d.

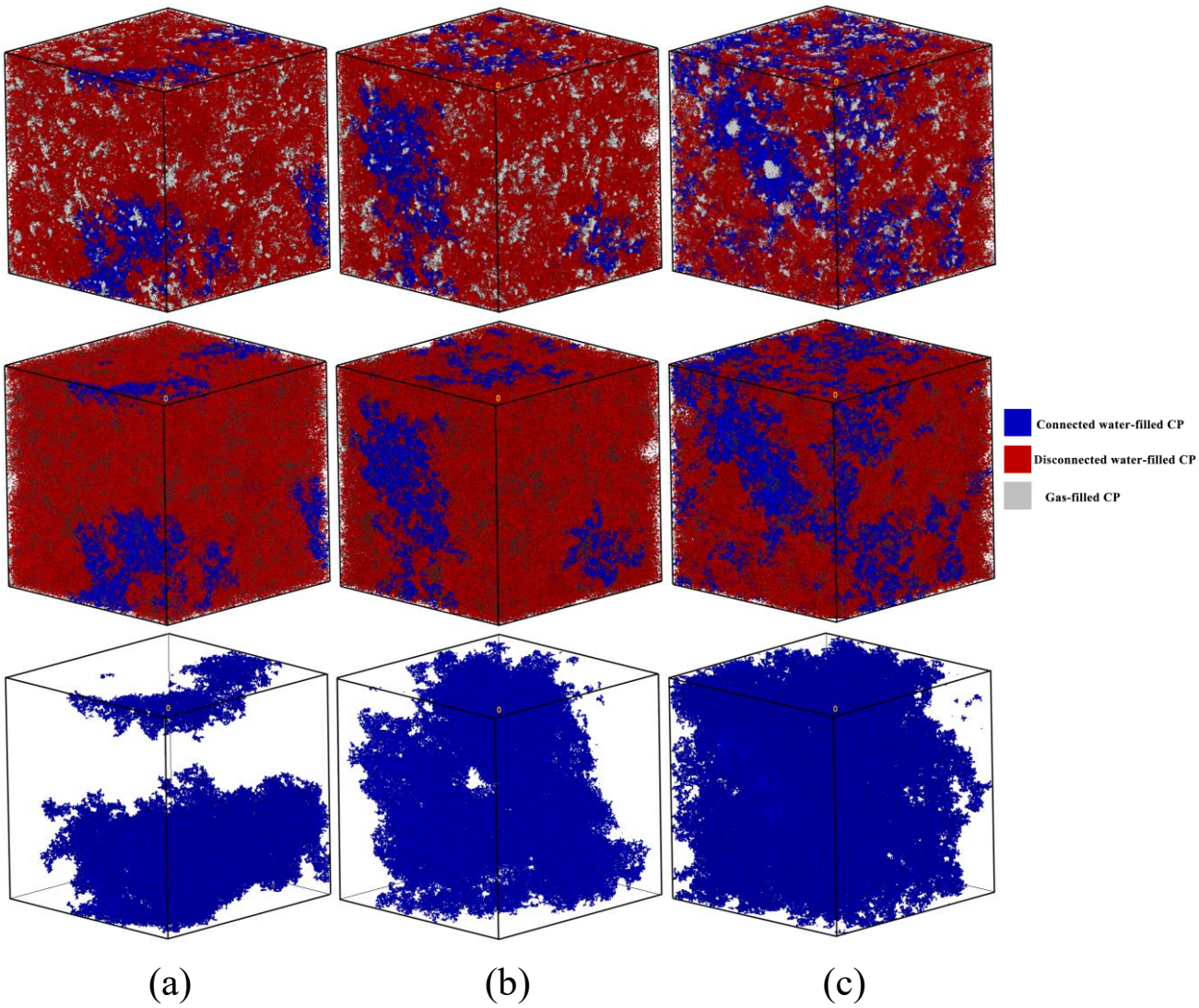

Fig. 17. Capillary pore structure consisting of gas-filled (grey), connected water-filled (blue), and disconnected water-filled capillary pores (red) in blended cement paste with 0% (a), 10% (b) and 20% 10% limestone powder (c), w/b ratio of 0.5, and degree of water saturation of 77% at 28 d.

Table 1 Chemical composition and physical properties of P.I. 52.5 Portland cement

Properties	Cement
Chemical composition (wt%)	
CaO	64.47
SiO_2	20.87
Al_2O_3	4.87
Fe_2O_3	3.59
MgO	2.13
SO_3	2.52
K_2O	0.65
Na_2O	0.11
Loss on ignition	0.77
Mineral components (vol%)	
C_3S	53.72
C_2S	24.09
C_3A	7.61
C_4AF	8.98
Physical properties	
Density (g/cm^3)	3.15
Fineness (m^2/kg)	369.6

Table 2 Summary of experimental studies on ionic diffusivity in saturated limestone blended cementitious materials.

Ref.	Binder	Specimen	w/b ratio	Porosity of paste	Curing condition	Test method
Hornain et al. [12]	PC, PC+20%LP	Paste, mortar	0.55	–	Kept 48 h at 20 °C and 100% RH and stored 60 d in water at 20 °C; 120 d for the entire duration of the test	Natural diffusion
Cam and Neithalath [14]	PC, PC+10%LP, PC+15%LP	Concrete	0.37,0.34	0.50, 0.39, 0.47, 0.45, 0.46, 0.39, 0.45, .0.40, 0.37, 0.34	Cured for 28 or 56 d in saturated curing conditions	Non-steady state migration
Tri Phung et al. [15]	PC, PC+10%LP, PC+20%LP	Paste	0.425, 0.375, 0.325	0.194, 0.168, 0.138	Cured in a temperature-controlled room at 22 ± 2 °C for 28 d	Natural diffusion
Li et al. [16]	PC, PC+30%LP, PC+40%LP, PC+50%LP	Concrete	0.3, 0.4, 0.5	0.167, 0.164, 0.176, 0.184, 0.185, 0.197	Cured in water for 28 d	Non-steady state migration